Stem Cell Reports
Article

ISSCR

OPEN ACCESS

# Proinflammatory phenotype of iPS cell-derived JAK2 V617F megakaryocytes induces fibrosis in 3D *in vitro* bone marrow niche

Niclas Flosdorf,[1,2,3,4] Janik Böhnke,[1,2,4] Marcelo A.S. de Toledo,[4,5] Niklas Lutterbach,[3] Vanesa Gómez Lerma,[1,2] Martin Graßhoff,[6] Kathrin Olschok,[4,5] Siddharth Gupta,[4,5] Vithurithra Tharmapalan,[2,4,7] Susanne Schmitz,[3] Katrin Götz,[3] Herdit M. Schüler,[8,9] Angela Maurer,[4,5] Stephanie Sontag,[1,2] Caroline Küstermann,[1,2] Kristin Seré,[1,2,3] Wolfgang Wagner,[2,4,7] Ivan G. Costa,[6] Tim H. Brümmendorf,[4,5] Steffen Koschmieder,[4,5] Nicolas Chatain,[4,5] Miguel Castilho,[10] Rebekka K. Schneider,[3] and Martin Zenke[1,2,4,5,*]

[1]Department of Cell Biology, Institute for Biomedical Engineering, RWTH Aachen University Medical School, Aachen, Germany
[2]Helmholtz Institute for Biomedical Engineering, RWTH Aachen University, Aachen, Germany
[3]Institute for Cell and Tumor Biology, RWTH Aachen University Medical School, Aachen, Germany
[4]Center for Integrated Oncology Aachen Bonn Cologne Düsseldorf (CIO ABCD), Aachen, Germany
[5]Department of Hematology, Oncology, Hemostaseology, and Stem Cell Transplantation, Faculty of Medicine, RWTH Aachen University Hospital, Aachen, Germany
[6]Institute of Computational Genomics, RWTH Aachen University Hospital, Aachen, Germany
[7]Institute for Stem Cell Biology, RWTH Aachen University Medical School, Aachen, Germany
[8]Institute for Human Genetics and Genome Medicine, Faculty of Medicine, RWTH Aachen University, Aachen, Germany
[9]Center for Rare Diseases, Medical Faculty, and University Hospital Düsseldorf Heinrich-Heine-University Düsseldorf, Düsseldorf, Germany
[10]Eindhoven University of Technology, Eindhoven, the Netherlands
*Correspondence: martin.zenke@rwth-aachen.de
https://doi.org/10.1016/j.stemcr.2023.12.011

## SUMMARY

The myeloproliferative disease polycythemia vera (PV) driven by the JAK2 V617F mutation can transform into myelofibrosis (post-PV-MF). It remains an open question how JAK2 V617F in hematopoietic stem cells induces MF. Megakaryocytes are major players in murine PV models but are difficult to study in the human setting. We generated induced pluripotent stem cells (iPSCs) from JAK2 V617F PV patients and differentiated them into megakaryocytes. In differentiation assays, JAK2 V617F iPSCs recapitulated the pathognomonic skewed megakaryocytic and erythroid differentiation. JAK2 V617F iPSCs had a TPO-independent and increased propensity to differentiate into megakaryocytes. RNA sequencing of JAK2 V617F iPSC-derived megakaryocytes reflected a proinflammatory, profibrotic phenotype and decreased ribosome biogenesis. In three-dimensional (3D) coculture, JAK2 V617F megakaryocytes induced a profibrotic phenotype through direct cell contact, which was reversed by the JAK2 inhibitor ruxolitinib. The 3D coculture system opens the perspective for further disease modeling and drug discovery.

## INTRODUCTION

Induced pluripotent stem cells (iPSCs) from patients represent an appealing resource to study malignant hematopoietic differentiation, elucidate molecular mechanisms of the cell types involved in disease onset, and test novel treatment regimens (Papapetrou, 2019; Yamanaka, 2020). Patient-specific iPSCs reflect the mutational background of the malignant clone and allow extensive expansion. This is key to modeling diseases *in vitro*, screening drugs, or studying cell types rarely found in patient specimens and to establish personalized treatment decisions.

Myeloproliferative neoplasms (MPNs) are a group of hematopoietic malignancies, including polycythemia vera (PV), essential thrombocytopenia (ET), and primary myelofibrosis (PMF) (Arber et al., 2016). The main driver mutation JAK2 V617F is prevalent in 50%–95% of MPN patients, depending on the subtype of the disease (Luque Paz et al., 2023; Vainchenker and Kralovics, 2017). The JAK2 V617F mutation initiates cytokine-independent constitutive downstream signaling in hematopoietic stem cells (HSCs) causing aberrant platelet production and red cell and myeloid proliferation (Mead and Mullally, 2017). Myelofibrosis (MF) can be either present at diagnosis in PMF or as a consequence of PV and ET (post-PV or post-ET MF) (Arber et al., 2016). In MF, hematopoiesis is replaced by extensive networks of fibers resembling scar formation in bone marrow (Tefferi, 2021). As a consequence, the bone marrow niche is disrupted, and megakaryocyte (MK) hyperplasia and clustering is pathognomonic for the disease. Currently, there is a lack of understanding as to why some patients progress to MF and what triggers this switch.

iPSCs capture the specific mutational landscape of JAK2 V617F PV patient cells. This entails comutations in *ASXL1*, *TET2*, and *EZH2* genes that improve the fitness of the aberrant hematopoietic clone (Grinfeld et al., 2018). iPSCs allow the study of these potentially subtle molecular and cellular differences. Previous research showed heterogeneity in the iPSC clones with JAK2 V617F mutation (Hosoi et al., 2014; Nilsri et al., 2021; Saliba et al., 2013; Ye et al.,

2014). Here, we generated iPSCs from a panel of JAK2 V617F PV patients and used CRISPR-Cas9 to establish isogenic controls to better understand this PV disease heterogeneity.

The majority of MPN patients are treated with cytoreductive therapies, and the only curative treatment is allogenic stem cell transplantation. Allogenic stem cell transplantation is, however, associated with significant morbidity and mortality (Gagelmann et al., 2022) and is thus reserved for patients with higher risk MF. Disease-modifying, antifibrotic treatments represent an urgent and unmet clinical need. Inhibitors of JAK2 (e.g., ruxolitinib) are the first-line treatment in intermediate risk MF, but have relatively modest effects on bone marrow fibrosis and the mutant clone (Kvasnicka et al., 2018; Verstovsek et al., 2017). It is crucial to understand the initiation of MF and how mutated MKs initiate the fibrotic transformation of fibrosis-driving mesenchymal stromal cells (MSCs) (Leimkühler et al., 2021). This should allow the development of new treatment options and also identify predictors for the phase transitions of PV toward post-PV-MF.

Human iPSCs can be differentiated into HSCs and various specialized blood cells by three-dimensional (3D) embryoid body (EB) formation (Ackermann et al., 2015; Ivanovs et al., 2017; Sturgeon et al., 2014). The addition of thrombopoietin (TPO) directs iPSC differentiation toward MKs and erythrocytes (Alsinet et al., 2022; Dalby et al., 2018; Lawrence et al., 2022; Liu et al., 2015). MKs represent only a small fraction of bone marrow cells, are not present in the peripheral blood, and are fragile to regular isolation methods (e.g., cell sorting), which makes them difficult to sample and study *in vitro*. Thus, there has been limited research on the interaction between fibrosis-driving MSCs and MKs (MSC-MK interaction) to date.

In recent years, it has become evident that MKs are involved in the initiation of MF in mouse models (i.e., through C-X-C motif ligand 4 [CXCL4]) (Gleitz et al., 2020; Leimkühler et al., 2021; Psaila et al., 2016, 2020), but a deeper understanding of the leading mechanism is lacking. The bone marrow niche is particularly difficult to mimic *in vitro* due to many components, such as vascular compartments, hematopoietic cells, stromal cells, bone, and extracellular matrix (ECM) components (e.g., collagen, other noncollagenous proteins such as fibronectin, laminin, and elastin). Only a few models have been developed thus far and have focused either on *in vivo* application (Grigoryan et al., 2022) or a broader approach that does not allow modifying the JAK2 V617F allele burden or cell types present (Khan et al., 2023).

We aimed to recapitulate the initiation of fibrosis by facilitating MSC-MK interactions in a 3D microfiber scaffold, which mimics the structure of the bone marrow *in vitro*. Here, we present patient-specific iPSCs from three PV patients and generated the complete repertoire of JAK2 V617F genotypes and CRISPR-Cas9-engineered isogenic controls. We demonstrate genotype-specific differences in MK cytokine secretion and profibrotic gene expression, which leads to the fibrotic activation of fibrosis-driving MSCs. This involves both soluble factors and direct MSC-MK interaction. Interestingly, ruxolitinib can inhibit the profibrotic MSC-MK interaction *in vitro*.

## RESULTS

### JAK2$^{V617F}$ iPSCs show altered hematopoietic differentiation as observed in patients

Patient-specific iPSCs were generated from peripheral blood mononuclear cells (PBMCs) from PV patients (1–3) with JAK2 V617F mutation (37%, 96% and 25% allele burden, respectively Tables 1 and S4). Nine clones were obtained with the genotypes JAK2 (no mutation), monoallelic JAK2 V617F mutation (JAK2$^{V617F/-}$), and biallelic JAK2 V617F mutation (JAK2$^{V617F/V617F}$). CRISPR-Cas9 was applied to JAK2$^{V617F/-}$ clones of patients 1 and 3, and patient 2 JAK2$^{V617F/V617F}$ clone to generate isogenic controls (Figures 1A and S1). The iPSC clones had the correct allelic status of JAK2 (chr9:g.5073770 [hg19], Exon 14, position 617), and the CRISPR-Cas9-edited clones contained additionally the silent mutation implemented in the donor template during editing (Tables S2 and S3). All of the iPSC clones were pluripotent and showed a normal karyotype and the expected DNA sequence at the *JAK2* locus (Figures S1–S3). The JAK2 V617F genotype of clones was confirmed by next-generation sequencing (NGS) and by PCR and Sanger sequencing. The iPSCs showed additional SNPs, but they were not classified as pathogenic or occurred in the normal population (Table 1). These SNPs affect *ASXL1* and *TP53* found in all patient iPSC clones. In patients 1 and 3 SNPs in *TET2*, *SETBP1*, and *CBL* were found. Patient 2 also had a SNP in *EZH2*. Only patient 2 progressed to MF later.

Since the discovery of the JAK2 V617F mutation in MPN patients, it became clear that it has a profound impact on hematopoiesis in terms of myeloid proliferation and clonal expansion (James et al., 2005; Kralovics et al., 2005). To investigate whether this has a similar impact *in vitro,* JAK2, JAK2$^{V617F/-}$, and JAK2$^{V617F/V617F}$ iPSCs were differentiated into hematopoietic cells adapting a protocol published by Liu et al. (2015) (Figures 1B–1E and S4A). EBs produced hematopoietic progenitor cells (CD34$^{+}$CD43$^{+}$; Figures S4B and S4C), erythrocytes (CD235a$^{+}$CD45$^{-}$; Figures 2A and 2B), and hemogenic endothelium-like cells (CD34$^{+}$CD43$^{-}$) as described previously (Satoh et al., 2021). In JAK2$^{V617F/V617F}$ cells, a significant increase in cell production for all of the patients was found (Figure 1C).

**Table 1. NGS analysis of patient-derived iPSCs**

| | Transcript | Location | c.HGSV | p.HGVS | Mutation class | JAK2 | JAK2$^{V617F/-}$ | JAK2$^{V617F/V617F}$ |
|---|---|---|---|---|---|---|---|---|
| Patient 1 | | | | | | | | |
| JAK2 | NM_004972 | E14 | c.1849G>T | p.Val617Phe | 5 | 0 | 48 | 100 |
| ASXL1 | NM_015338 | E12 | c.2444T>C | p.Leu815Pro | 1 | 100 | 100 | 100 |
| CBL | NM_005188 | E9 | c.1380_1382dup | p.Asp460dup | 2 | 43 | 46 | 42 |
| MPL | NM_005373 | E3 | c.340G>A | p.Val114Met | 1 | 47 | 50 | 48 |
| SETBP1 | NM_015559 | E4 | c.691G>C | p.Val231Leu | 1 | 99 | 100 | 100 |
| SH2B3 | NM_005475 | E3 | c.784T>C | p.Trp262Arg | 1 | n.a. | 51 | 50 |
| TET2 | NM_001127208 | E11 | c.5284A>G | p.Ile1762Val | 2 | 49 | 49 | 52 |
| TP53 | NM_000546 | E4 | c.215C>G | p.Pro72Arg | 2 | 49 | 59 | 51 |
| Patient 2 | | | | | | | | |
| JAK2 | NM_004972 | E14 | c.1849G>T | p.Val617Phe | 5 | 0 | 52 | 99 |
| ASXL1 | NM_015338 | E12 | c.2444T>C | p.Leu815Pro | 1 | 100 | 100 | 100 |
| EZH2 | NM_004456 | E6 | c.553G>C | p.Asp185His | 1 | 53 | 51 | 51 |
| TP53 | NM_000546 | E4 | c.215C>G | p.Pro72Arg | 2 | 100 | 100 | 99 |
| Patient 3 | | | | | | | | |
| JAK2 | NM_004972 | E14 | c.1849G>T | p.Val617Phe | 5 | 0 | 39 | 100 |
| ASXL1 | NM_015338 | E12 | c.2444T>C | p.Leu815Pro | 1 | 100 | 100 | 100 |
| SETBP1 | NM_015559 | E4 | c.3301G>A | p.Val1101Ile | 1 | 49 | 51 | 50 |
| TET2 | NM_001127208 | E11 | c.5284A>G | p.Ile1762Val | 2 | 49 | 50 | 50 |
| TP53 | NM_000546 | E4 | c.215C>G | p.Pro72Arg | 2 | 53 | 52 | 50 |

Genomic DNA of patient-derived iPSCs was analyzed for 31 or 32 MPN-related genes with NGS (see also supplemental information). For all of the detected nonsynonymous variants, the transcript affected, the type of mutation on DNA and protein level, and their classification in disease (5: pathogenic, 4: likely pathogenic, 3: uncertain, 2: likely not pathogenic or of little clinical significance, and 1: not pathogenic or of no clinical significance) are listed. c.HGVS and p.HGVS, DNA coding and protein coding variants, respectively, defined by the Human Genome Variation Society (HGVS); n.a., not analyzed.

CD61$^+$CD41$^+$ MKs were prominently observed in all differentiations in the presence of TPO. More important, patient 2, who developed post-PV-MF, showed a significant increase in the CD61$^+$CD41$^+$ population in the JAK2$^{V617F/-}$ and JAK2$^{V617F/V617F}$ clones (Figures 2C and 2D). For the CD61$^+$ MK population, Romanowsky staining and imaging confirmed MK features, such as pro-platelet formation. Transmission electron microscopy (TEM) images revealed a demarcation membrane system and granules (Figures 1B, 1D, and 1E). iPSC clones from patients 1 and 3 (no progression to MF) did not have a significant increase in CD61$^+$CD41$^+$ cells derived from JAK2$^{V617F/-}$ and JAK2$^{V617F/V617F}$ iPSCs compared to JAK2 iPSCs without mutation.

A prominent CD235a$^+$CD45$^-$ population was observed after differentiating patient 2 JAK2$^{V617F/-}$ and JAK2$^{V617F/V617F}$ iPSCs into hematopoietic cells (Figures 2A, 2B, 2E, and 2F). This was a significant increase compared to the JAK2 clone without mutation of the same patient. Of note, the JAK2 V617F-associated erythrocytosis was observed independent of erythropoietin (EPO), similar to iPSC lines from patients with a high JAK2 V617F allele burden established previously (Ye et al., 2014). t-Distributed stochastic neighbor embedding (tSNE) analysis of flow cytometry data of CD31, CD34, CD41, CD42b, CD43, CD45, CD61, and CD235a, including data from all three patients and the respective isogenic controls, revealed a coexpression of progenitor markers CD31 and CD34 with the MK markers CD41 and CD61 Figure S4C), highlighting a strong MK differentiation commitment in progenitor cells. JAK2$^{V617F/V617F}$ and JAK2$^{V617F/-}$ cells showed distinct CD45$^-$CD235$^+$ clusters, which did not appear for JAK2 cells without mutation (Figure 2E). Taken together, these results indicate that the iPSC clones recapitulate the malignant

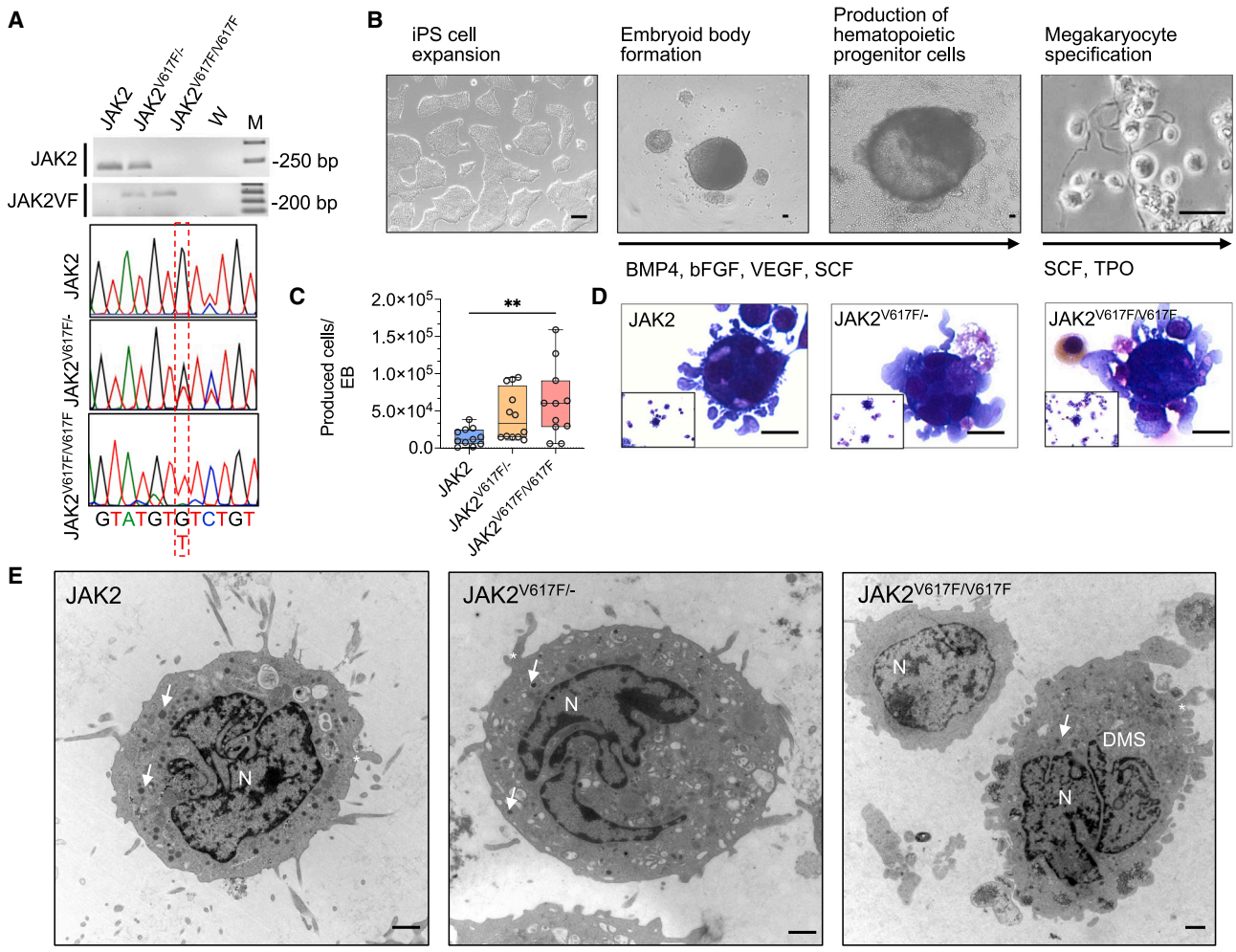


**Figure 1. Patient-derived JAK2$^{V617F/-}$ and JAK2$^{V617F/V617F}$ iPSC differentiation into MKs**

(A) Representative allele-specific PCR analysis and Sanger sequencing of iPSCs without JAK2 mutation and monoallelic and biallelic JAK2 V617F mutation (JAK2, JAK2$^{V617F/-}$, and JAK2$^{V617F/V617F}$, respectively). The G>T transition in JAK2 V617F mutated clones is indicated. W, water control.

(B) iPSC differentiation into EBs, hematopoietic progenitors, and MKs by specific cytokines as indicated.

(C) JAK2 V617F mutation increased the total cell numbers produced per EB (day 14) of all 3 patients. Each dot represents an independent experiment (n = 11–12).

(D) The iPSC-MKs showed MK morphology with budding and proplatelet formation (Romanowski staining, patient 2). Scale bars, 50 μm.

(E) Images of iPSC-MKs by TEM (patient 2). DMS, demarcation membrane system; N, nucleus. Asterisks indicate proplatelet protrusions. White arrows mark granules. Scale bars, 1,000 nm.

See also Figures S1–S3.

and skewed hematopoiesis observed in the patient from whom they originated.

## MK differentiation in JAK2$^{V617F}$ iPSCs is TPO independent

TPO is the main effector of the cytokine receptor MPL (myeloproliferative leukemia protein). Activated MPL drives megakaryopoiesis and platelet production, which relies on JAK2 (Sangkhae et al., 2014). The addition of TPO to the differentiation of JAK2 iPSCs from patient 2 enhanced the frequency of CD61$^{+}$CD41$^{+}$ cells significantly (Figures 3A and 3B). This effect, however, was less prominent in JAK2$^{V617F/-}$ iPSCs with an increase of only 7.3% induced by TPO. The JAK2$^{V617F/-}$ iPSCs already produced similar amounts of CD61$^{+}$CD41$^{+}$ cells without TPO as JAK2 iPSCs in the presence of TPO and also significantly more CD61$^{+}$CD41$^{+}$ cells compared to unstimulated JAK2 cells. JAK2$^{V617F/V617F}$ iPSCs produce significantly more CD61$^{+}$CD41$^{+}$ cells compared to unstimulated JAK2 cells, without an additional effect of TPO. A similar trend was

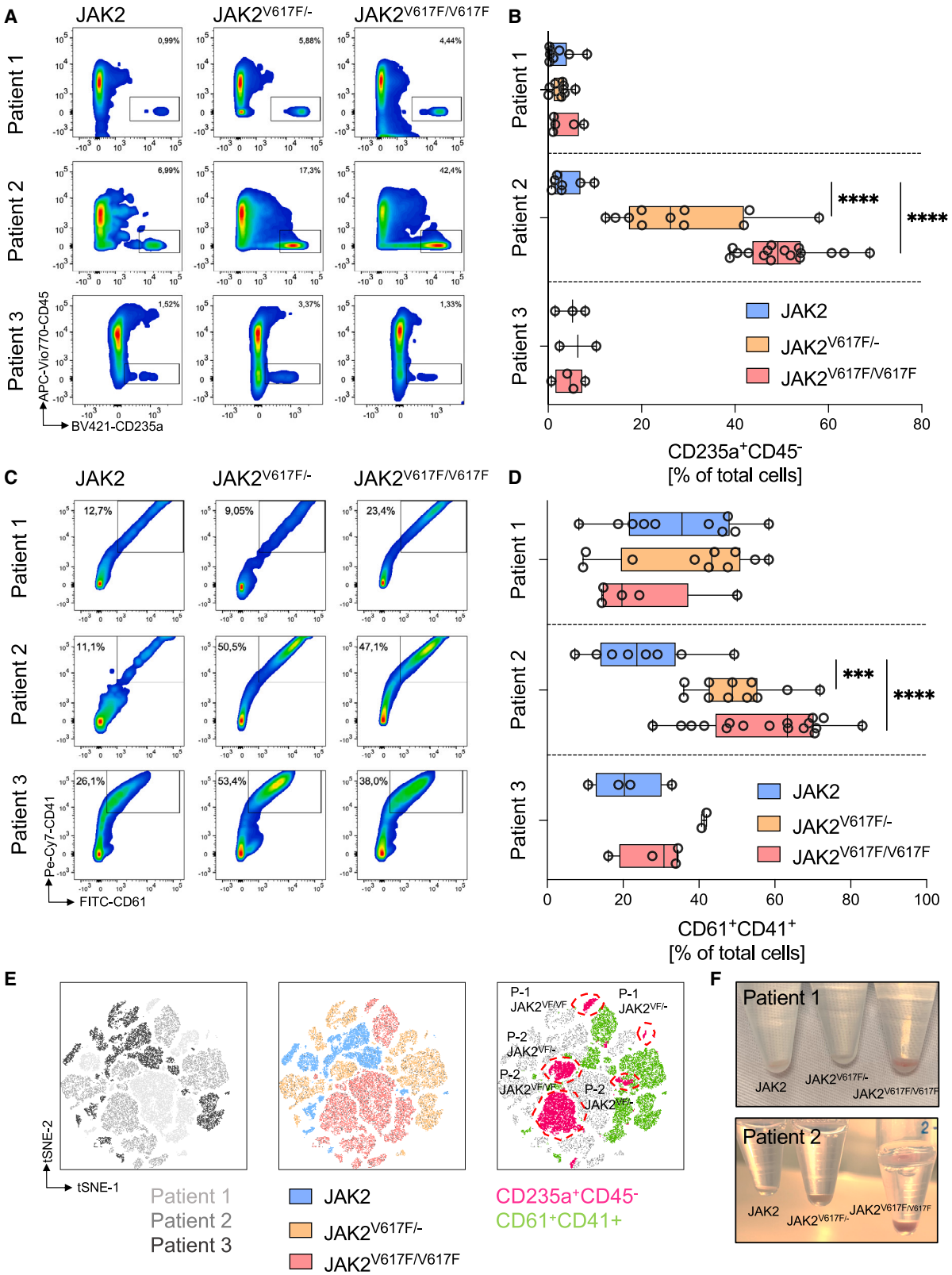


*(legend on next page)*

observed when looking at the $CD41^+CD42b^+$ cells (Figures 3A and 3B).

## $JAK2^{V617F/V617F}$ MKs exhibit a proinflammatory signature

Based on the prominent PV-like phenotype during differentiation, we proceeded to interrogate patient 2 $JAK2^{V617F/V617F}$ MKs and JAK2 controls by performing bulk RNA sequencing of $CD61^+$ cells (day 14 of differentiation) (Figure 2C). A total of 279 significantly differentially expressed genes (92 downregulated and 187 upregulated genes, respectively) were detected between the genotypes (Figures 4A and 4B). CIBERSORT was applied, which imputes gene expression profiles and provides an estimation of the abundances of member cell types in a mixed cell population (Newman et al., 2015). This analysis confirmed a high similarity of iPSC-derived MKs to primary MKs *in vivo* (Mills and Krantz, 2018) (GSE119828) (Figure 4C).

Next, we applied PROGENy to identify signaling pathway–responsive genes based on publicly available perturbation experiments and DoRothEA to identify differentially regulated transcription factors (TFs) (Garcia-Alonso et al., 2019; Schubert et al., 2018). As expected, the JAK2 pathway was activated in $JAK2^{V617F/V617F}$ MKs compared to controls, which was also visible by pronounced activation of genes in the *STAT1* network (Figures 4D and 4E). Indicative of a proinflammatory and profibrotic phenotype and in line with *in vivo* observations, V617F mutated MKs showed upregulation of hypoxia 1a (HIF1A), tumor necrosis factor alpha (TNF-α) and the transforming growth factor β (TGF-β) pathways (Figure 4D). The most downregulated genes in $JAK2^{V617F/V617F}$ MKs were *COL1A1* and *COL3A1*, with other structural proteins, such as *FN1*, *COL4A1*, *COL4A2*, and *COL5A1*, also among the top 20 (Figure S5A). Gene Ontology (GO) terms for collagen were also among the most significantly downregulated terms in $JAK2^{V617F/V617F}$ MKs (Figure S5B). The most upregulated genes were complement C3b/C4b receptor 1-like (*CR1L*) and *HIF1A-AS3* (Figure S5A).

To gain more information about the effect of both of the JAK2 V617F mutations in MKs and the global gene expression changes, we applied gene set enrichment analysis (GSEA) (Mootha et al., 2003; Subramanian et al., 2005). An abundant chemokine profile in $JAK2^{V617F/V617F}$ MKs was detected. A ribosome-associated gene set was enriched in JAK2 $CD61^+$ cells without mutation (Figures 4F and 4G); hence, fewer ribosome associated genes were found in $JAK2^{V617F/V617F}$ MKs. The cytokine *CXCL8* (also known as interleukin-8 [IL-8]) was most prominently upregulated, a feature also visible in PMF patient iPSCs (Hosoi et al., 2014). The increased *CXCL8* expression was accompanied by increased CXCL8 secretion measured in a cytokine array (Figure 4H). Other cytokines that were secreted at high levels in $JAK2^{V617F/V617F}$ MKs were monocyte chemoattractant protein-1 (MCP-1), IL-6, growth-related oncogene (GRO), tissue inhibitor of metalloproteinases metallopeptidase inhibitor-1 (TIMP-1), osteopontin, neutrophil activating protein-2 (NAP-2) , GRO-a, and epithelial neutrophil-activating protein-78 (ENA-78), some previously described to be upregulated in MPN patient blood (Obro et al., 2020; Pardanani et al., 2011; Verachi et al., 2022). Transcripts of these cytokines were also found to be more strongly enriched in JAK2 V617F MKs (data not shown).

We observed pronounced inflammatory and profibrotic signatures and a decrease in structural proteins in JAK2 V617F $CD61^+$ cells, potentially related to the altered maturation of MKs in MPN (Balduini et al., 2011). In particular, our gene expression study reveals activation of the HIF1A locus in accord with previous findings (Baumeister et al., 2020).

## Impaired protein synthesis in $JAK2^{V617F/V617F}$ MKs

In $JAK2^{V617F/V617F}$ MKs, the gene set ribosome biogenesis (GO: 0042254) was significantly negative enriched (Figures 4F and 4G). Previous studies showed that in PMF the activation of the JAK/STAT signaling leads to ribosomal protein small subunit 14 (*RPS14*) deficiency, directly influencing the ribosome (Ling et al., 2018). To show that there was an effect on the protein synthesis in $JAK2^{V617F/V617F}$ MKs, we measured the incorporation of OP-Puro in iPSC-MKs during protein synthesis and found a reduction in $JAK2^{V617F/V617F}$ MKs (Figure 4I). Thus, the MKs from PV

**Figure 2. Hematopoietic differentiation of $JAK2^{V617F/-}$ and $JAK2^{V617F/V617F}$ iPSCs recapitulates skewed myeloid differentiation of PV patients**

(A and B) Increased erythropoiesis of patient 2 iPSCs with JAK2 V617F mutation in MK differentiation (day 14) independent of EPO by increased frequency of $CD235a^+CD45^-$ cells in flow cytometry.

(C and D) Production of $CD61^+CD41^+$ MKs for all iPSC clones of all of the patients, which was particularly prominent for the JAK2 V617F mutated cells of patient 2.

(E) tSNE analysis of events from all 3 patients revealed more prominent clusters of $CD235a^+CD45^-$ cells overlapping especially with the $JAK2^{V617F/-}$ and $JAK2^{V617F/V617F}$ cells (patients 1 and 2).

(F) Increased erythropoiesis in $JAK2^{V617F/V617F}$ cells as evidenced by red cell pellet at day 14 of differentiation as in (A)–(E).

(B and D) Each dot represents an independent experiment (patient 1, n = 5–10; patient 2, n = 7–17; patient 3, n = 2–4).

See also Figure S4.

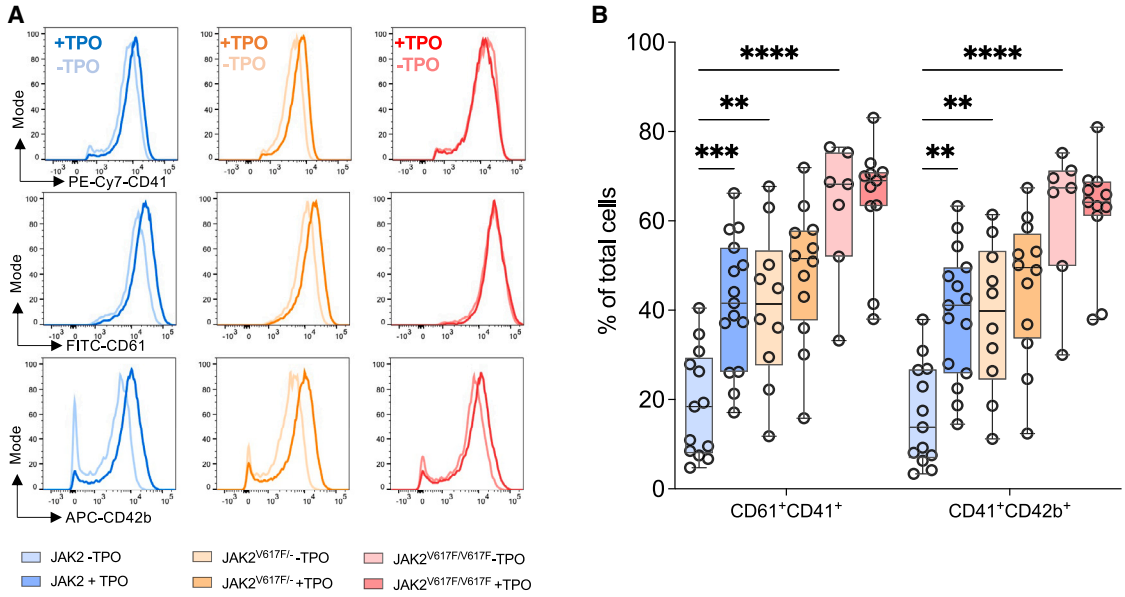


**Figure 3. JAK2$^{V617F/-}$ and JAK2$^{V617F/V617F}$ iPSCs develop into MKs independently of TPO**

(A) Flow cytometry analysis (CD41, CD42b, CD61) of JAK2 V617F MKs of patient 2 in response to TPO (2 days) on day 14 of MK differentiation shows independence of TPO in JAK2$^{V617F/V617F}$ cells.

(B) Quantification of CD61$^+$CD41$^+$ and CD41$^+$CD42b$^+$ cells in response of TPO as in (A) of patients 1–3. JAK2$^{V617F/V617F}$ depicts data of patient 2. JAK2 V617F cells show TPO independent increased production of MKs, whereas MK production of unmutated cells was TPO dependent. Each dot represents an independent experiment (JAK2, n = 13–15; JAK2$^{V617F/-}$, n = 10–12; JAK2$^{V617F/V617F}$, n = 5–11).

patients mimic main features of other MPN model systems, such as GATA$^{low}$ mice, describing a correlation between the mutation, decreased ribosome biogenesis, and translation. This finding is of particular interest because reduced protein synthesis has been linked to proinflammatory but not yet to profibrotic phenotypes. In addition, *RPS14* deficiency was shown to have an impact on MK and erythroid differentiation (Schneider et al., 2016).

## MSC-MK JAK2$^{V617F}$ coculture recapitulates MF features

Next, we explored the profibrotic phenotype of JAK2$^{V617F}$ MKs. Conventional 2D coculture of MKs with MSC on tissue culture plastic did not induce profibrotic gene expression, such as ACTA2/α2-smooth muscle actin (Figure S6A; data not shown). Three-dimensional culture systems are known to better mimic the bone marrow niche functionality in terms of hematopoietic support (Bourgine et al., 2018) than 2D models and would therefore provide a more faithful recapitulation of fibrotic transformation in MF. To investigate the impact of JAK2$^{V617F}$ MKs on MF, iPSC-derived MKs were cocultured with primary or immortalized bone marrow MSCs (Bourgine et al., 2017) for 72 h on a fiber-based scaffold produced by melt electrowriting (MEW) technology (Castilho et al., 2018, 2019) (Figures 5A and 5B). This scaffold was chosen to facilitate cell infiltration and better approximate the complex bone marrow niche ECM fiber environment.

iPSC-derived CD61$^+$ MKs of patients 1 and 2 were used for coculture with MSCs (Figure 5A), one of whom transformed to MF (patient 2). The presence and interaction of MKs and MSCs on the scaffold was analyzed by GFP (MSCs) and immunofluorescence staining of CD42b (MKs) (Figure 5C). CD42b$^+$ MKs were located in close proximity to GFP$^+$ MSC. Following coculture in scaffolds for 3 days, MSCs were isolated from scaffold and subjected to RNA expression analysis (Figures 5D and S6B–S6D).

MSCs cocultured with JAK2$^{V617F/V617F}$ MKs upregulated the fibrotic marker genes *ACTA2*, *FAP*, and *GLI1* significantly compared to a coculture with JAK2 MKs without mutation (Figures 5D, S6C, and S6D). Moreover, *TGF-β1* and *COL1A1* expression was also increased in MSCs, but the increase of *COL1A1* expression was not statistically significant. JAK2$^{V617F/-}$ MKs induced a similar but not as prominent trend of upregulation. A coculture with conditioned medium of CD61$^+$ MKs (supernatant) did have similar effects on *GLI1* but not on *ACTA2* or *FAP* (Figures S6E–S6G). Thus, the induction of fibrotic marker genes appears not to be fully mediated by soluble factors but requires direct MSC-MK contact. In summary, because MKs have been attributed a major role in the development of bone marrow fibrosis *in vivo* (Gleitz et al., 2020; Kramann and Schneider, 2018), it was reassuring to observe similar effects in our *in vitro* model.

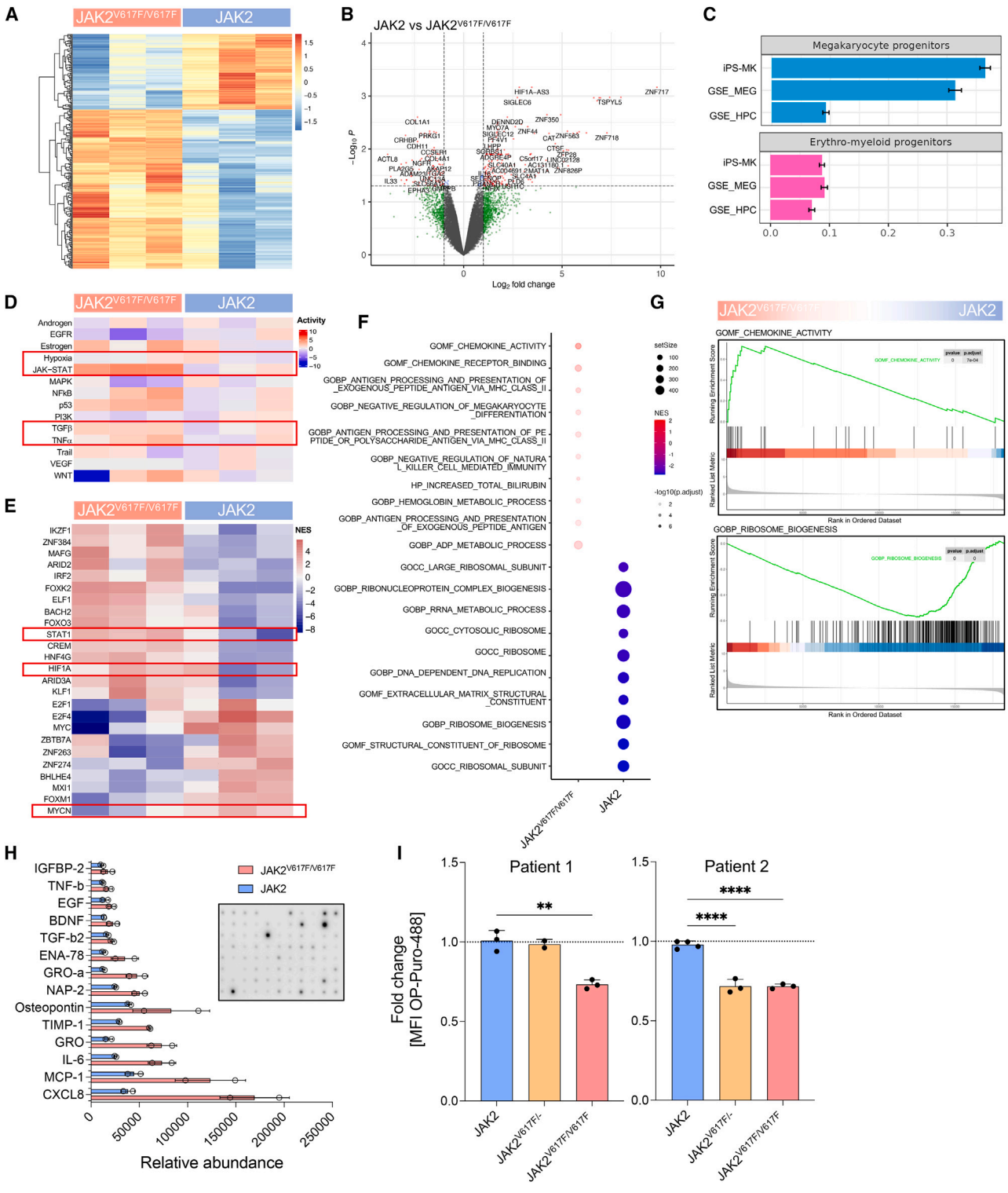


**Figure 4. JAK2$^{V617F/V617F}$ iPS MKs express an inflammatory gene signature**

iPSCs with homozygous JAK2 V617F mutation and without mutation were differentiated into MKs (day 14) and subjected to bulk RNA sequencing analysis (N = 3, patient 2).

(A and B) JAK2$^{V617F/V617F}$ MKs showed 279 significantly differentially expressed genes (187 downregulated and 92 upregulated genes, respectively) and are represented in heatmap and volcano plot format (A and B, respectively).

*(legend continued on next page)*

### Perturbation of iPSC-MK-induced fibrosis by ruxolitinib

The JAK2 inhibitor ruxolitinib can reverse or delay bone marrow fibrosis in patients (Kvasnicka et al., 2018). Therefore, to further extend the MSC-MK JAK2$^{V617F/V617F}$ coculture experiments, we performed perturbations by pharmacological intervention using ruxolitinib. The profibrotic effect of JAK2$^{V617F/V617F}$ MKs was ameliorated or almost abolished when 1 μM ruxolitinib was added to coculture (Figure 5D). Ruxolitinib alone had no effect on MSC and on coculture of MSC and JAK2 MKs without mutation (Figures S6H and S6I). MSC stimulated by JAK2$^{V617F/V617F}$ MKs also expressed less of the HSC supporting cytokine *CXCL12*, but this effect was not reversed by ruxolitinib (Figure 5D).

Previous work in mouse models demonstrated the impact of CXCL4 in MF (Gleitz et al., 2020). To assess the activity of CXCL4 on MK-induced fibrosis in our 3D coculture system, *CXCL4* knockout MKs were used (Boehnke et al., 2021). JAK2$^{V617F/-}$ *CXCL4* knockout MKs caused low *GLI1* expression in MSC but left profibrotic gene expression unaffected (Figure S6J). This may be because CXCL4 action on profibrotic genes requires an additional cell type, which is not present in the MSC-MK coculture system.

In summary, we observe that ruxolitinib abolished the upregulation of fibrotic markers, thereby paving the way to use the 3D MSC-MK coculture system for drug screening.

## DISCUSSION

HSCs driven by JAK2 V617F cause PV, which can progress in MF, and MKs were shown as major players of MF in murine models. Here, we generated a panel of JAK2 V617F iPSCs from PV patients and differentiated them in MKs. We developed a 3D MSC-MK coculture system to mimic the MF bone marrow niche. The iPSC-derived MKs showed the intrinsic differences between JAK2 V617F genotypes and patient-specific features. This highlights the advantages of the iPSC model to capture the patient-specific genetic profile and mutational landscape, including comutations, which correlate with clinical outcomes in MPN (Grinfeld et al., 2018; Luque Paz et al., 2023).

We differentiated homozygous and heterozygous JAK2 V617F iPSCs and isogenic controls into MKs. JAK2 V617F iPSCs of all patients matured from progenitors into MKs independently of TPO. Patient 2 exhibited a particularly high JAK2 V617F allele burden (97%) and transformed to MF. Interestingly, Saliba et al. (2013) reported on a PV patient with homozygous JAK2 V617F mutation and high allele burden (99%) who progressed to MF and thus exhibited the same genotype, similar high allele burden, and disease progression as patient 2. JAK2 V617F iPSCs of patient 2 showed a strong propensity to develop CD235a$^{+}$ erythrocytes independently of EPO, which is in accordance with a prevalence of hyperplastic erythropoiesis in JAK2 V617F PV patients with high allele burden. Which factors contribute to an increased erythropoiesis in PV (Levine and Gilliland, 2008) and in PV iPS cells remains an open question, as shown here. Overexpression of JAK2 V617F alone in iPSCs showed modest effects on erythropoiesis (Liu et al., 2023; Nilsri et al., 2021). In JAK2 V617F PV patients and JAK2 V617F knockin mice loss of heterozygosity through uniparental disomy of 9p24, where JAK2 is located, is supposed to correlate with the switch to increased erythropoiesis (Li et al., 2014).

The properties of patient 2 JAK2 V617F iPSCs and the diseased cells derived thereof emphasize the impact of the iPSC approach chosen here to captures the patient's genomic profile, including thus-far unknown and potentially disease-relevant mutations. We can expect with the advance of molecular profiling of PV by NGS (Luque Paz et al., 2023) to get to know more about the genetic predisposition, disease-associated mutations, and molecular mechanism involved.

JAK2 V617F MKs showed a skewed gene expression profile toward cytokines involved in inflammation and MF (e.g., CXCL8/IL-8, MCP-1, TNF-α, TGF-β) in accordance with other studies (Fleischman et al., 2011; Hosoi et al., 2014; Olschok et al., 2021). In addition, JAK2 V617F MKs induced aspects of fibrosis in MSCs shown by the

(C) CIBERSORT analysis identified iPSC-MKs of all genotypes as MK and erythromyeloid progenitors (GSE_Meg and GSE_HPC refer to MK and hematopoietic progenitor [HPC] datasets).
(D) PROGENy analysis revealed prominent upregulation of the JAK-STAT and also upregulation of hypoxia, TNF-α, and TGF-β pathways (red boxes).
(E) DoRothEA analysis showed downregulation of TFs MYCN and upregulation STAT1 and HIF1A (red boxes).
(F and G) GSEA analysis showed, among others, the positive enrichment of chemokines and the negative enrichment of ribosome-associated genes.
(H) ELISA of multiple chemokines shows prominent upregulation of inflammatory cytokines in JAK2$^{V617F/V617F}$ MKs (CXCL8/IL-8, MCP-1, IL-6).
(I) Uptake of OP-Puro in nascent peptide chains was decreased in JAK2$^{V617F/V617F}$ MKs (patients 1 and 2; n = 2–3 and n = 3–4, respectively).
See also Figure S5.

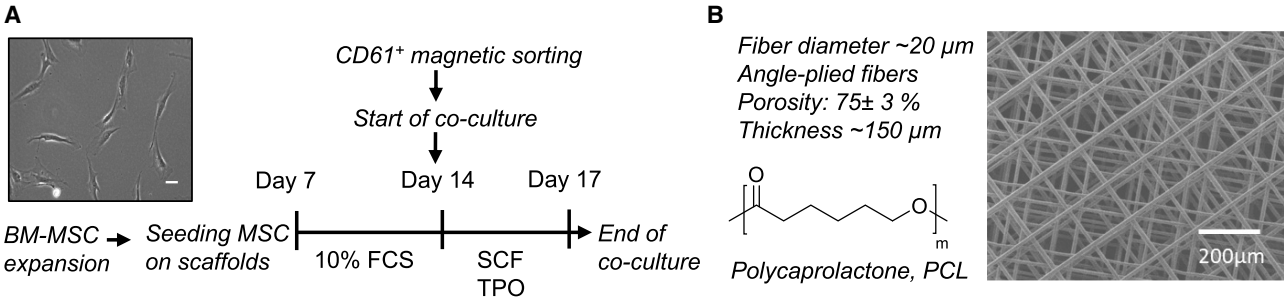


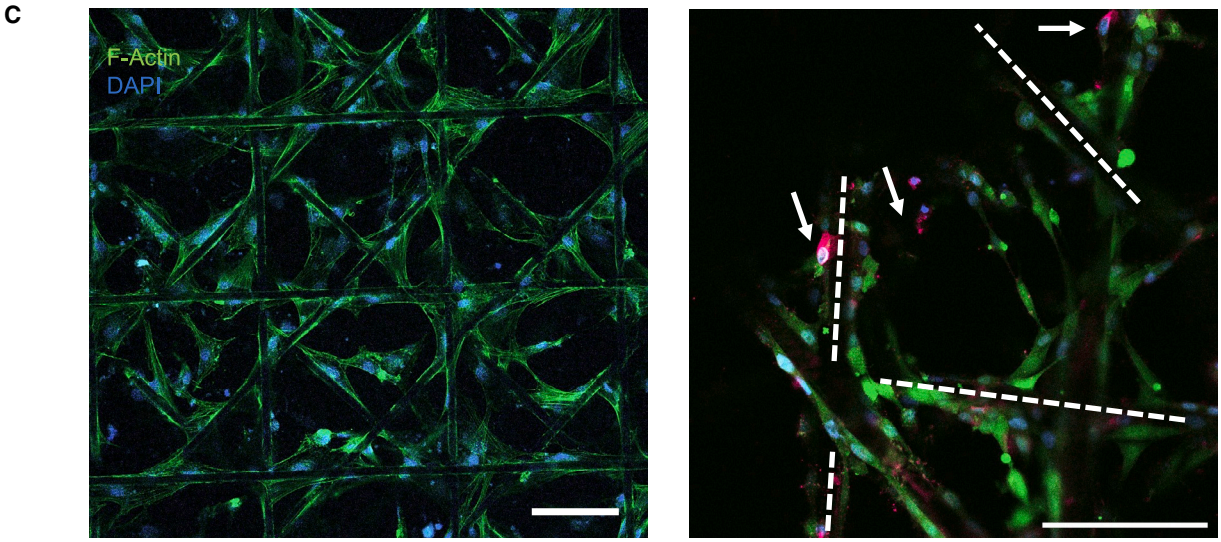


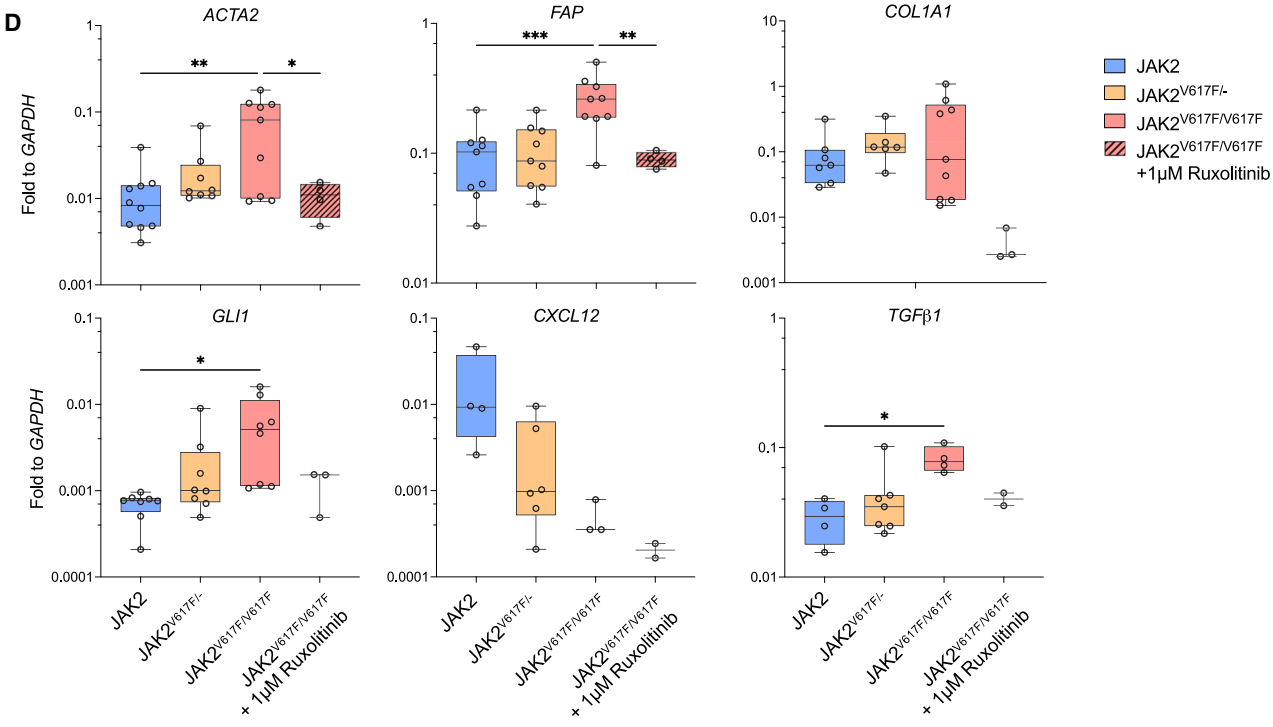


(legend on next page)

upregulation of fibrosis marker genes, such as *ACTA2* and *FAP*. More important, this was genotype specific and independent of the individual patient and not observed with unmutated MKs. Interestingly, JAK2 V617F MKs decreased hematopoietic support as indicated by lower *CXCL12* expression in MSCs, thus recapitulating another hallmark of MF (Kramann and Schneider, 2018).

The JAK2 inhibitor ruxolitinib showed an impact on erythrocyte differentiation in JAK2 V617F mutated iPSCs (Ye et al., 2014). In our study in 3D MSC-MK coculture, ruxolitinib compromised the upregulation of fibrosis markers in JAK2$^{V617F/V617F}$ MKs but not MKs without mutation or MSCs only. This shows that our 3D coculture platform is highly suitable for screening drugs *in vitro* for the inhibition of MK-induced fibrosis. In this context, we note that so far ruxolitinib had only minor effects on fibrosis in patients (Kvasnicka et al., 2018; Oh et al., 2022). This may be because the inhibition of additional signaling pathways further to JAK2 signaling, such as nuclear factor-κB (NF-κB) signaling, are required to treat fibrosis, as demonstrated in mouse models (Kleppe et al., 2018).

Previous work showed that *CXCL4* knockout reduces fibrosis *in vivo* (Gleitz et al., 2020), which was thus far not observed in our coculture system. In addition, Hoeft et al. (2023) demonstrated that platelet-derived CXCL4 stimulates macrophages to polarize and drive fibrosis in a mouse model of myocardial infarction. Thus, to gain further insights into MKs driving fibrosis, we envision the addition of further cell types with a potential role in fibrosis to advance our 3D coculture model. The strength of our coculture platform is to allow individual fine-tuning of parameters, such as using a defined stromal compartment and cells with a defined genotype and allele burden. These features are not present in other coculture platforms presented so far (Khan et al., 2023). Microfiber scaffolds have already proven to be useful for cartilage tissue regeneration (Castilho et al., 2019) and allowed us to approximate a bone marrow–like environment for the culture of MSCs.

In summary, we show that the JAK2 V617F mutation in iPSCs from PV patients recapitulates myeloid proliferation. MKs with homozygous JAK2 V617F mutation have the potential to initiate fibrosis. Our 3D coculture platform allowed us to study the induction of fibrosis by JAK2$^{V617F/V617F}$ MKs and should permit exploring novel treatment options. The 3D coculture platform is expected to serve as a valuable tool to further investigate novel drug candidates and/or gain further insights into MSC-MK interactions and PV disease progression toward MF.

## EXPERIMENTAL PROCEDURES

### Resource availability

#### *Corresponding author*

Further information and requests for resources and reagents should be directed to and will be fulfilled by the corresponding author.

#### *Materials availability*

iPSCs generated in this study will be made available on request, but may require a completed Materials Transfer Agreement.

#### *Data and code availability*

The data discussed in this publication have been deposited in NCBI's Gene Expression Omnibus and are accessible through GEO: GSE228092. (https://www.ncbi.nlm.nih.gov/geo/query/acc.cgi?acc=GSE228092).

### Patient-specific iPSCs with JAK2 V617F mutation

Patient-specific iPSCs were reprogrammed from PBMCs of three PV patients (referred to as patient 1, patient 2, and patient 3) with JAK2 V617F mutation after written informed consent (local ethics board reference no. EK206/09) using *OCT4*, *SOX2*, *c-MYC*, and *KLF4* in CytoTune Sendai virus vectors (Thermo Fisher Scientific, Waltham, MA) as described (Boehnke et al., 2021; Satoh et al., 2021; Sontag et al., 2017). iPSCs with monoallelic and biallelic JAK2 V617F mutation (JAK2$^{V617F/-}$ and JAK2$^{V617F/V617F}$) and without mutation were isolated. For patient 2 (JAK2 V617F allele burden 96%), only JAK2$^{V617F/V617F}$ iPSC clones were obtained. For patients 1 and 3 (JAK2 V617F allele burden of 37% and 25%, respectively) JAK2 and JAK2$^{V617F/-}$ iPSC clones were obtained. JAK2$^{V617F/-}$ and JAK2$^{V617F/V617F}$ iPSCs and isogenic controls per patient were generated by CRISPR-Cas9 editing (IDT, Coralville, IA). Routinely, iPSCs were maintained in StemMACS iPS-Brew XF on 6-well plates coated with Matrigel (Corning, Corning, NY).

### iPSC differentiation into MKs and 3D culture with MSC

Differentiation of human iPSCs into MKs was done by a spin EB protocol (Liu et al., 2015) with some modifications, as described in Satoh et al. (2021) and Olschok et al. (2021). Primary MSCs from the femoral heads of hip replacement surgeries (local ethics board reference no. EK300/13) or the immortalized MSC line

**Figure 5. JAK2$^{V617F/-}$ and JAK2$^{V617F/V617F}$ MKs induce profibrotic gene expression in stromal cells in a 3D coculture model**

(A) Schematic representation of coculturing MSCs and MKs on 3D scaffolds.

(B) Representative scanning electron microscopy image of MEW printed fiber scaffolds with respective scaffold characteristics.

(C) MSC growing on the scaffolds (left) and in coculture (right). JAK2 V617F MKs (CD42b, arrows) were in close proximity to MSC (GFP).

(D) ACTA2, FAP, GLI1, COL1A1, and TGF-β1 gene expression in MSC was upregulated in coculture with JAK2 V617F MKs and CXCL12 gene expression was downregulated (patients 1 and 2). Ruxolitinib treatment abolished the activity of JAK2$^{V617F/V617F}$ MKs. Each dot represents an independent experiment (JAK2, n = 4–10; JAK2$^{V617F/-}$, n = 6–9; JAK2$^{V617F/V617F}$, n = 3–9; ruxolitinib, n = 2–4).

See also Figure S6.

MSOD (Bourgine et al., 2017) were obtained from human bone marrow and seeded on polycaprolactone (PCL) MEW scaffolds (Figure 5B) at a density of $2 \times 10^5$ cells/cm$^2$ scaffold and cultured in α-MEM (Cytiva, Marlborough, MA) supplemented with 10% fetal calf serum (Capricorn, Ebsdorfergrund, Germany), 100 U/mL penicillin and 100 μg/mL streptomycin, 2 mM glutamine, 10 mM HEPES, and 1 mM sodium pyruvate (all Thermo Fisher Scientific). In cocultures $2 \times 10^5$ CD61$^+$ iPSC-MKs (day 14) were added to 3D cultured MSC on MEW scaffolds in serum free medium (SFM) containing the corresponding cytokines. Half- medium changes were performed daily, and MKs and MSC were cocultured for 3 days.

### Flow cytometric analysis of hematopoietic differentiation

Cells were analyzed by flow cytometry as described by Olschok et al. (2021) and Toledo et al. (2021) (Figure S4B; Table S1) and analyzed with FACS Canto II or LSR Fortessa and FlowJo software (all BD Bioscience, Franklin Lakes, NJ). For the analysis of protein biosynthesis with flow cytometry, the protein synthesis assay kit (ab239725, Abcam, Cambridge, UK) was used.

Diff-Quik staining cells were centrifuged onto glass slides in the Cytospin 4 cytocentrifuge (Thermo Fisher Scientific). Cells were fixed with methanol, stained with Diff-Quik (Medion Diagnostics, Düdingen, Switzerland), and mounted with Entellan (Merck, Rahway, NJ).

### Statistical analysis

Statistical analyses were performed in Prism 9 (GraphPad, San Diego, CA) using one-way or two-way ANOVA with Tukey's multiple comparisons test or Dunnett's multiple comparisons test. Results were reported as follows: 0.1234 (ns), 0.0332 (*), 0.0021 (**), 0.0002 (***), <0.0001 (****) with specific comparisons as indicated in the respective figure legends.

### Additional methods

Detailed description of CRISPR-Cas9 editing of iPSCs, iPSC differentiation into MKs, immunofluorescence staining, Epi-PluriScore, TEM, NGS and cytogenetic analysis, gene expression analysis by qRT-PCR and RNA sequencing, ELISA analysis, and MEW of fiber scaffolds are contained in the supplemental information.

## SUPPLEMENTAL INFORMATION

Supplemental information can be found online at https://doi.org/10.1016/j.stemcr.2023.12.011.

## ACKNOWLEDGMENTS

We thank Carmen Schalla for their technical assistance with protein biochemistry. We also thank Ivan Martin, University of Basel, for kindly providing immortalized MSCs (MSOD) for the coculture experiments. Parts of the experiments were supported by the Interdisciplinary Center for Clinical Research Aachen (IZKF Aachen, Medical Faculty, RWTH Aachen) FACS Core Facility and the Genomics Facility. Biomaterial samples for iPSC reprogramming were derived from the RWTH centralized Biomaterial Bank Aachen (RWTH cBMB, Aachen, Germany) in accordance with the regulations of the biomaterial bank and the approval of the ethics committee of the Medical Faculty, RWTH Aachen University, Aachen, Germany. This work was supported in part by funds from the German Research Foundation (Deutsche Forschungsgemeinschaft; DFG) to N.C. and M.Z. (428858617), R.K.S. (417911533), W.W. (428857589 and 417911533), I.G.C. (428857561), and S.K. (428858786) as part of the Clinical Research Unit (CRU344). R.K.S. and I.C.G. were funded by the Fibromap Consortia of the Federal Ministry of Education and Research, Germany. M.C. is grateful for financial support from the Reprint Project (OCENW.XS5.161) of The Netherlands Organization for Scientific Research. R.K.S. is an Oncode Institute investigator and supported by a European Research Council (ERC) grant (deFIBER; ERC-StG 757339). M.A.S.d.T. was funded by a CAPES-Alexander von Humboldt postdoctoral fellowship (99999.001703/2014-05) and a donation by U. Lehmann. V.G.L. was supported by a fellowship of the Erasmus European Union student exchange program. Parts of this work were generated within the PhD theses of J.B. and N.F. at RWTH Aachen University, Aachen, Germany.

## AUTHOR CONTRIBUTIONS

N.F. designed and performed experiments and wrote the manuscript. J.B., M.A.S.d.T., N.L., V.G.L., K.O., and S.G. designed and performed RNA sequencing, ELISA, or hematopoietic differentiation experiments and provided support for the data analyses. V.T. and W.W. performed DNA methylation analyses. H.M.S. performed the cytogenetic analyses. A.M. performed the NGS analyses. S. Sontag, C.K., K.S., S. Schmitz, and K.G. performed experiments on iPSC generation, culture, and differentiation. M.G. and I.G.C. analyzed and interpreted the data. S.K., N.C., and T.H.B. provided patient samples and support for the data analyses and interpretation. M.C. printed the PCL scaffolds and provided support on the design of the experiments. R.K.S. and M.Z. designed the experiments, analyzed the data, and wrote the manuscript. All of the authors approved the final version of the manuscript for submission.

## DECLARATION OF INTERESTS

W.W. and V.T. are involved in Cygenia GmbH (www.cygenia.com), which provides services for DNA methylation analysis to other scientists. S.K. reports funding from Novartis, Bristol-Myers Squibb, and Janssen/Geron; advisory board honoraria from Pfizer, Incyte, Ariad, Novartis, AOP Pharma, BMS, Celgene, Geron, Janssen, CTI, Roche, Baxalta, GSK, Sierra Oncology, and Sanofi; a patent for Bromodomain and Extra-Terminal (BET) inhibitor at RWTH Aachen University; honoraria from Novartis, Bristol Myers Squibb, Celgene, Geron, Janssen, Pfizer, Incyte, Ariad, Shire, Roche, and AOP Pharma; and other financial support (e.g., travel support) from Alexion, Novartis, Bristol Myers Squibb, Incyte, Ariad, AOP Pharma, Baxalta, CTI, Pfizer, Sanofi, Celgene, Shire, Janssen, Geron, Abbvie, Imago Biosciences, Sierra Oncology, GSK, and Karthos. T.H.B. served as a consultant for Janssen, Merck, Novartis, and Pfizer; received research funding form Novartis and Pfizer; and received honoraria from Janssen, Merck, Novartis, and Pfizer.

Received: April 6, 2023
Revised: December 22, 2023
Accepted: December 26, 2023
Published: January 25, 2024

## REFERENCES


Ackermann, M., Liebhaber, S., Klusmann, J.H., and Lachmann, N. (2015). Lost in translation: pluripotent stem cell-derived hematopoiesis. EMBO Mol. Med. *7*, 1388–1402.

Alsinet, C., Primo, M.N., Lorenzi, V., Bello, E., Kelava, I., Jones, C.P., Vilarrasa-Blasi, R., Sancho-Serra, C., Knights, A.J., Park, J.E., et al. (2022). Robust temporal map of human in vitro myelopoiesis using single-cell genomics. Nat. Commun. *13*, 2885.

Arber, D.A., Orazi, A., Hasserjian, R., Thiele, J., Borowitz, M.J., Le Beau, M.M., Bloomfield, C.D., Cazzola, M., and Vardiman, J.W. (2016). The 2016 revision to the World Health Organization classification of myeloid neoplasms and acute leukemia. Blood *127*, 2391–2405.

Balduini, A., Badalucco, S., Pugliano, M.T., Baev, D., De Silvestri, A., Cattaneo, M., Rosti, V., and Barosi, G. (2011). In vitro megakaryocyte differentiation and proplatelet formation in Ph-negative classical myeloproliferative neoplasms: distinct patterns in the different clinical phenotypes. PLoS One *6*, e21015.

Baumeister, J., Chatain, N., Hubrich, A., Maié, T., Costa, I.G., Denecke, B., Han, L., Küstermann, C., Sontag, S., Seré, K., et al. (2020). Hypoxia-inducible factor 1 (HIF-1) is a new therapeutic target in JAK2V617F-positive myeloproliferative neoplasms. Leukemia *34*, 1062–1074.

Boehnke, J., Atakhanov, S., Toledo, M.A.S., Schüler, H.M., Sontag, S., Chatain, N., Koschmieder, S., Brümmendorf, T.H., Kramann, R., and Zenke, M. (2021). CRISPR/Cas9 mediated CXCL4 knockout in human iPS cells of polycythemia vera patient with JAK2 V617F mutation. Stem Cell Res. *55*, 102490.

Bourgine, P.E., Gaudiello, E., Pippenger, B., Jaquiery, C., Klein, T., Pigeot, S., Todorov, A., Feliciano, S., Banfi, A., and Martin, I. (2017). Engineered extracellular matrices as biomaterials of tunable composition and function. Adv. Funct. Mater. *27*.

Bourgine, P.E., Klein, T., Paczulla, A.M., Shimizu, T., Kunz, L., Kokkaliaris, K.D., Coutu, D.L., Lengerke, C., Skoda, R., Schroeder, T., and Martin, I. (2018). In vitro biomimetic engineering of a human hematopoietic niche with functional properties. Proc. Natl. Acad. Sci. USA *115*, E5688–E5695.

Castilho, M., Hochleitner, G., Wilson, W., van Rietbergen, B., Dalton, P.D., Groll, J., Malda, J., and Ito, K. (2018). Mechanical behavior of a soft hydrogel reinforced with three-dimensional printed microfibre scaffolds. Sci. Rep. *8*, 1245.

Castilho, M., Mouser, V., Chen, M., Malda, J., and Ito, K. (2019). Bilayered micro-fibre reinforced hydrogels for articular cartilage regeneration. Acta Biomater. *95*, 297–306.

Dalby, A., Ballester-Beltrán, J., Lincetto, C., Mueller, A., Foad, N., Evans, A., Baye, J., Turro, E., Moreau, T., Tijssen, M.R., and Ghevaert, C. (2018). Transcription factor levels after forward programming of human pluripotent stem cells with GATA1, FLI1, and TAL1 determine megakaryocyte versus erythroid cell fate decision. Stem Cell Reports *11*, 1462–1478.

Fleischman, A.G., Aichberger, K.J., Luty, S.B., Bumm, T.G., Petersen, C.L., Doratotaj, S., Vasudevan, K.B., LaTocha, D.H., Yang, F., Press, R.D., et al. (2011). TNFalpha facilitates clonal expansion of JAK2V617F positive cells in myeloproliferative neoplasms. Blood *118*, 6392–6398.

Gagelmann, N., Wolschke, C., Salit, R.B., Schroeder, T., Ditschkowski, M., Panagiota, V., Cassinat, B., Thol, F., Badbaran, A., Robin, M., et al. (2022). Reduced intensity hematopoietic stem cell transplantation for accelerated-phase myelofibrosis. Blood Adv. *6*, 1222–1231.

Garcia-Alonso, L., Holland, C.H., Ibrahim, M.M., Turei, D., and Saez-Rodriguez, J. (2019). Benchmark and integration of resources for the estimation of human transcription factor activities. Genome Res. *29*, 1363–1375.

Gleitz, H.F.E., Dugourd, A.J.F., Leimkühler, N.B., Snoeren, I.A.M., Fuchs, S.N.R., Menzel, S., Ziegler, S., Kröger, N., Triviai, I., Büsche, G., et al. (2020). Increased CXCL4 expression in hematopoietic cells links inflammation and progression of bone marrow fibrosis in MPN. Blood *136*, 2051–2064.

Grigoryan, A., Zacharaki, D., Balhuizen, A., Côme, C.R., Garcia, A.G., Hidalgo Gil, D., Frank, A.K., Aaltonen, K., Mañas, A., Esfandyari, J., et al. (2022). Engineering human mini-bones for the standardized modeling of healthy hematopoiesis, leukemia, and solid tumor metastasis. Sci. Transl. Med. *14*, eabm6391.

Grinfeld, J., Nangalia, J., Baxter, E.J., Wedge, D.C., Angelopoulos, N., Cantrill, R., Godfrey, A.L., Papaemmanuil, E., Gundem, G., MacLean, C., et al. (2018). Classification and personalized prognosis in myeloproliferative neoplasms. N. Engl. J. Med. *379*, 1416–1430.

Hoeft, K., Schaefer, G.J.L., Kim, H., Schumacher, D., Bleckwehl, T., Long, Q., Klinkhammer, B.M., Peisker, F., Koch, L., Nagai, J., et al. (2023). Platelet-instructed SPP1+ macrophages drive myofibroblast activation in fibrosis in a CXCL4-dependent manner. Cell Rep. *42*, 112131.

Hosoi, M., Kumano, K., Taoka, K., Arai, S., Kataoka, K., Ueda, K., Kamikubo, Y., Takayama, N., Otsu, M., Eto, K., et al. (2014). Generation of induced pluripotent stem cells derived from primary and secondary myelofibrosis patient samples. Exp. Hematol. *42*, 816–825.

Ivanovs, A., Rybtsov, S., Ng, E.S., Stanley, E.G., Elefanty, A.G., and Medvinsky, A. (2017). Human haematopoietic stem cell development: from the embryo to the dish. Development *144*, 2323–2337.

James, C., Ugo, V., Le Couédic, J.P., Staerk, J., Delhommeau, F., Lacout, C., Garçon, L., Raslova, H., Berger, R., Bennaceur-Griscelli, A., et al. (2005). A unique clonal JAK2 mutation leading to constitutive signalling causes polycythaemia vera. Nature *434*, 1144–1148.

Khan, A.O., Rodriguez-Romera, A., Reyat, J.S., Olijnik, A.A., Colombo, M., Wang, G., Wen, W.X., Sousos, N., Murphy, L.C., Grygielska, B., et al. (2023). Human bone marrow organoids for disease modeling, discovery, and validation of therapeutic targets in hematologic malignancies. Cancer Discov. *13*, 364–385.

Kleppe, M., Koche, R., Zou, L., van Galen, P., Hill, C.E., Dong, L., De Groote, S., Papalexi, E., Hanasoge Somasundara, A.V., Cordner, K., et al. (2018). Dual targeting of oncogenic activation and inflammatory signaling increases therapeutic efficacy in myeloproliferative neoplasms. Cancer Cell *33*, 29–43.e7.

Kralovics, R., Passamonti, F., Buser, A.S., Teo, S.-S., Tiedt, R., Passweg, J.R., Tichelli, A., Cazzola, M., and Skoda, R.C. (2005). A Gain-of-Function Mutation of JAK2 in Myeloproliferative Disorders. N. Engl. J. Med. *352*, 1779–1790.

Kramann, R., and Schneider, R.K. (2018). The identification of fibrosis-driving myofibroblast precursors reveals new therapeutic avenues in myelofibrosis. Blood *131*, 2111–2119.

Kvasnicka, H.M., Thiele, J., Bueso-Ramos, C.E., Sun, W., Cortes, J., Kantarjian, H.M., and Verstovsek, S. (2018). Long-term effects of ruxolitinib versus best available therapy on bone marrow fibrosis in patients with myelofibrosis. J. Hematol. Oncol. *11*, 42.

Lawrence, M., Shahsavari, A., Bornelöv, S., Moreau, T., McDonald, R., Vallance, T.M., Kania, K., Paramor, M., Baye, J., Perrin, M., et al. (2022). Mapping the biogenesis of forward programmed megakaryocytes from induced pluripotent stem cells. Sci. Adv. *8*, eabj8618.

Leimkühler, N.B., Gleitz, H.F.E., Ronghui, L., Snoeren, I.A.M., Fuchs, S.N.R., Nagai, J.S., Banjanin, B., Lam, K.H., Vogl, T., Kuppe, C., et al. (2021). Heterogeneous bone-marrow stromal progenitors drive myelofibrosis via a druggable alarmin axis. Cell Stem Cell *28*, 637–652.e8.

Levine, R.L., and Gilliland, D.G. (2008). Myeloproliferative disorders. Blood *112*, 2190–2198.

Li, J., Kent, D.G., Godfrey, A.L., Manning, H., Nangalia, J., Aziz, A., Chen, E., Saeb-Parsy, K., Fink, J., Sneade, R., et al. (2014). JAK2V617F homozygosity drives a phenotypic switch in myeloproliferative neoplasms, but is insufficient to sustain disease. Blood *123*, 3139–3151.

Ling, T., Crispino, J.D., Zingariello, M., Martelli, F., and Migliaccio, A.R. (2018). GATA1 insufficiencies in primary myelofibrosis and other hematopoietic disorders: consequences for therapy. Expert Rev. Hematol. *11*, 169–184.

Liu, C., Imai, M., Edahiro, Y., Mano, S., Takei, H., Nudejima, M., Kurose, A., Morishita, S., Ando, M., Tsuneda, S., et al. (2023). Establishment of isogenic induced pluripotent stem cells with or without pathogenic mutation for understanding the pathogenesis of myeloproliferative neoplasms. Exp. Hematol. *118*, 12–20.

Liu, Y., Wang, Y., Gao, Y., Forbes, J.A., Qayyum, R., Becker, L., Cheng, L., and Wang, Z.Z. (2015). Efficient generation of megakaryocytes from human induced pluripotent stem cells using food and drug administration-approved pharmacological reagents. Stem Cells Transl. Med. *4*, 309–319.

Luque Paz, D., Kralovics, R., and Skoda, R.C. (2023). Genetic basis and molecular profiling in myeloproliferative neoplasms. Blood *141*, 1909–1921.

Mead, A.J., and Mullally, A. (2017). Myeloproliferative neoplasm stem cells. Blood *129*, 1607–1616.

Mills, J.A., and Krantz, I.D. (2018). Genome-wide Transcriptome Analysis of NIPBL Hematopoeitic Progenitors and Megakaryocytes. https://www.ncbi.nlm.nih.gov/geo/query/acc.cgi?acc=GSE119828.

Mootha, V.K., Lindgren, C.M., Eriksson, K.F., Subramanian, A., Sihag, S., Lehar, J., Puigserver, P., Carlsson, E., Ridderstråle, M., Laurila, E., et al. (2003). PGC-1alpha-responsive genes involved in oxidative phosphorylation are coordinately downregulated in human diabetes. Nat. Genet. *34*, 267–273.

Newman, A.M., Liu, C.L., Green, M.R., Gentles, A.J., Feng, W., Xu, Y., Hoang, C.D., Diehn, M., and Alizadeh, A.A. (2015). Robust enumeration of cell subsets from tissue expression profiles. Nat. Methods *12*, 453–457.

Nilsri, N., Jangprasert, P., Pawinwongchai, J., Israsena, N., and Rojnuckarin, P. (2021). Distinct effects of V617F and exon12-mutated JAK2 expressions on erythropoiesis in a human induced pluripotent stem cell (iPSC)-based model. Sci. Rep. *11*, 5255.

Øbro, N.F., Grinfeld, J., Belmonte, M., Irvine, M., Shepherd, M.S., Rao, T.N., Karow, A., Riedel, L.M., Harris, O.B., Baxter, E.J., et al. (2020). Longitudinal cytokine profiling identifies GRO-alpha and EGF as potential biomarkers of disease progression in essential thrombocythemia. Hemasphere *4*, e371.

Oh, S.T., Verstovsek, S., Gotlib, J., Gupta, V., Platzbecker, U., Gisslinger, H., Devos, T., Kiladjian, J.-J., McLornan, D.P., Perkins, A.C., et al. (2022). Bone marrow fibrosis changes do not correlate with efficacy outcomes in myelofibrosis: analysis of more than 300 JAK inhibitor-naïve patients treated with momelotinib or ruxolitinib. Blood *140*, 821–823.

Olschok, K., Han, L., de Toledo, M.A.S., Böhnke, J., Graßhoff, M., Costa, I.G., Theocharides, A., Maurer, A., Schüler, H.M., Buhl, E.M., et al. (2021). CALR frameshift mutations in MPN patient-derived iPSCs accelerate maturation of megakaryocytes. Stem Cell Rep. *16*, 2768–2783.

Papapetrou, E.P. (2019). Modeling myeloid malignancies with patient-derived iPSCs. Exp. Hematol. *71*, 77–84.

Pardanani, A., Begna, K., Finke, C., Lasho, T., and Tefferi, A. (2011). Circulating levels of MCP-1, sIL-2R, IL-15, and IL-8 predict anemia response to pomalidomide therapy in myelofibrosis. Am. J. Hematol. *86*, 343–345.

Psaila, B., Barkas, N., Iskander, D., Roy, A., Anderson, S., Ashley, N., Caputo, V.S., Lichtenberg, J., Loaiza, S., Bodine, D.M., et al. (2016). Single-cell profiling of human megakaryocyte-erythroid progenitors identifies distinct megakaryocyte and erythroid differentiation pathways. Genome Biol. *17*, 83.

Psaila, B., Wang, G., Rodriguez-Meira, A., Li, R., Heuston, E.F., Murphy, L., Yee, D., Hitchcock, I.S., Sousos, N., O'Sullivan, J., et al. (2020). Single-Cell Analyses Reveal Megakaryocyte-Biased Hematopoiesis in Myelofibrosis and Identify Mutant Clone-Specific Targets. Mol. Cell *78*, 477–492.e8.

Saliba, J., Hamidi, S., Lenglet, G., Langlois, T., Yin, J., Cabagnols, X., Secardin, L., Legrand, C., Galy, A., Opolon, P., et al. (2013). Heterozygous and Homozygous JAK2V617F States Modeled by Induced Pluripotent Stem Cells from Myeloproliferative Neoplasm Patients. PLoS One *8*, 742577–e74312.

Sangkhae, V., Etheridge, S.L., Kaushansky, K., and Hitchcock, I.S. (2014). The thrombopoietin receptor, MPL, is critical for development of a JAK2V617F-induced myeloproliferative neoplasm. Blood *124*, 3956–3963.

Satoh, T., Toledo, M.A.S., Boehnke, J., Olschok, K., Flosdorf, N., Götz, K., Küstermann, C., Sontag, S., Seré, K., Koschmieder, S., et al. (2021). Human DC3 antigen presenting dendritic cells from induced pluripotent stem cells. Front. Cell Dev. Biol. *9*, 667304.

Schneider, R.K., Schenone, M., Ferreira, M.V., Kramann, R., Joyce, C.E., Hartigan, C., Beier, F., Brümmendorf, T.H., Germing, U., Platzbecker, U., et al. (2016). Rps14 haploinsufficiency causes a block in erythroid differentiation mediated by S100A8 and S100A9. Nat. Med. *22*, 288–297.

Schubert, M., Klinger, B., Klünemann, M., Sieber, A., Uhlitz, F., Sauer, S., Garnett, M.J., Blüthgen, N., and Saez-Rodriguez, J. (2018). Perturbation-response genes reveal signaling footprints in cancer gene expression. Nat. Commun. *9*, 20.

Sontag, S., Förster, M., Qin, J., Wanek, P., Mitzka, S., Schüler, H.M., Koschmieder, S., Rose-John, S., Seré, K., and Zenke, M. (2017). Modelling IRF8 deficient human hematopoiesis and dendritic cell development with engineered iPS cells. Stem Cell. *35*, 898–908.

Sturgeon, C.M., Ditadi, A., Awong, G., Kennedy, M., and Keller, G. (2014). Wnt signaling controls the specification of definitive and primitive hematopoiesis from human pluripotent stem cells. Nat. Biotechnol. *32*, 554–561.

Subramanian, A., Tamayo, P., Mootha, V.K., Mukherjee, S., Ebert, B.L., Gillette, M.A., Paulovich, A., Pomeroy, S.L., Golub, T.R., Lander, E.S., and Mesirov, J.P. (2005). Gene set enrichment analysis: a knowledge-based approach for interpreting genome-wide expression profiles. Proc. Natl. Acad. Sci. USA *102*, 15545–15550.

Tefferi, A. (2021). Primary myelofibrosis: 2021 update on diagnosis, risk-stratification and management. Am. J. Hematol. *96*, 145–162.

Toledo, M.A.S., Gatz, M., Sontag, S., Gleixner, K.V., Eisenwort, G., Feldberg, K., Hamouda, A.E.I., Kluge, F., Guareschi, R., Rossetti, G., et al. (2021). Nintedanib targets KIT D816V neoplastic cells derived from induced pluripotent stem cells of systemic mastocytosis. Blood *137*, 2070–2084.

Vainchenker, W., and Kralovics, R. (2017). Genetic basis and molecular pathophysiology of classical myeloproliferative neoplasms. Blood *129*, 667–679.

Verachi, P., Gobbo, F., Martelli, F., Martinelli, A., Sarli, G., Dunbar, A., Levine, R.L., Hoffman, R., Massucci, M.T., Brandolini, L., et al. (2022). The CXCR1/CXCR2 inhibitor reparixin alters the development of myelofibrosis in the Gata1 (low) mice. Front. Oncol. *12*, 853484.

Verstovsek, S., Gotlib, J., Mesa, R.A., Vannucchi, A.M., Kiladjian, J.J., Cervantes, F., Harrison, C.N., Paquette, R., Sun, W., Naim, A., et al. (2017). Long-Term survival in patients treated with ruxolitinib for myelofibrosis: COMFORT-I and-II pooled analyses. J. Hematol. Oncol. *10*, 156.

Yamanaka, S. (2020). Pluripotent stem cell-based cell therapy-promise and challenges. Cell Stem Cell *27*, 523–531.

Ye, Z., Liu, C.F., Lanikova, L., Dowey, S.N., He, C., Huang, X., Brodsky, R.A., Spivak, J.L., Prchal, J.T., and Cheng, L. (2014). Differential sensitivity to JAK inhibitory drugs by isogenic human erythroblasts and hematopoietic progenitors generated from patient-specific induced pluripotent stem cells. Stem Cell. *32*, 269–278.